# Effect of Temperature Dependent Fluid Properties on Heat Transfer in Turbulent Mixed Convection

**Francesco Zonta**[1]
e-mail: francesco.zonta@uniud.it

**Alfredo Soldati**[1]
e-mail: soldati@uniud.it

Center for Fluid Mechanics and Hydraulics,
DiEGM, University of Udine,
Udine 33100, Italy

*The effect of the uniform fluid properties approximation (Oberbeck-Boussinesq (OB)) in turbulent mixed convection is investigated via direct numerical simulation (DNS) of water flows with viscosity ($\mu$) and thermal expansion coefficient ($\beta$) both independently and simultaneously varying with temperature (non-Oberbeck-Boussinesq conditions (NOB)). Mixed convection is analyzed for the prototypical case of Poiseuille-Rayleigh-Bénard (PRB) turbulent channel flow. In PRB flows, the combination of buoyancy driven (Rayleigh-Bénard) with pressure driven (Poiseuille) effects produce a complex flow structure, which depends on the relative intensity of the flow parameters (i.e., the Grashof number, Gr, and the shear Reynolds number, $Re_\tau$). In liquids, however, temperature variations induce local changes of fluid properties which influence the macroscopic flow field. We present results for different absolute values of the shear Richardson numbers ($Ri_\tau = |Gr/Re_\tau^2|$) under constant temperature boundary conditions. As $Ri_\tau$ is increased buoyant thermal plumes are generated, which induce large scale thermal convection that increases momentum and heat transport efficiency. Analysis of friction factor ($C_f$) and Nusselt number (Nu) for NOB conditions shows that the effect of viscosity is negligible, whereas the effect of thermal expansion coefficient is significant. Statistics of mixing show that (i) mixing increases for increasing $Ri_\tau$ (and decreases for increasing $Re_\tau$) and (ii) the effect of thermal expansion coefficient on mixing increases for increasing $Ri_\tau$ (and decreases for increasing $Re_\tau$). A simplified phenomenological model to predict heat transfer rates in PRB flows has also been developed.* [DOI: 10.1115/1.4025135]

*Keywords: DNS, turbulence, heat transfer, mixed convection, temperature dependent fluid properties*

## 1 Introduction

In industrial applications, buoyancy effects (induced by either density/temperature gradients) in pressure driven turbulent flows (PRB flows) increase mixing and heat transfer rates due to large-scale circulation [1]. In a number of such situations, natural convection phenomena influence the forced convection effects, originating mixed convection flows. These flows are also important in geophysical instances such as oceanic circulation [2]. Compared to forced convection, large scale circulation phenomena (large vortices whose characteristic dimension scales with the domain size) alter the dynamics of turbulence transport mechanism near a wall: turbulent diffusion transfers turbulent kinetic energy (TKE) from the near-wall region to the outer region, whereas velocity-pressure gradient correlation transfers TKE produced by buoyancy in the convective layer toward the near-wall region [3].

Turbulent PRB flows are usually investigated under the OB approximation (fluid properties are independent of temperature). However, PRB flows often occur in the presence of large temperature gradients, which may induce significant variation of fluid properties, namely of fluid viscosity ($\mu$) and thermal expansion coefficient ($\beta$) [4]. From a practical standpoint, it is important to quantify the influence of non-Oberbeck-Boussinesq assumptions on the computation of transfer rates [5,6]. Benchmarking the importance of NOB-related fluid behavior can be also important for studies in which fluid properties are artificially modified to increase heat transfer coefficient [7–9].

The sole effect of buoyancy on wall-bounded flows in the absence of the mean shear (Rayleigh-Bénard convection) has been extensively investigated both experimentally (see Ahlers et al. [10], for a review) and numerically [11,12]. By contrast, PRB turbulent channel flow has received little attention compared to its practical importance. Experimental works on PRB flows were performed by Komori et al. [13], Fukui and Nakajima [14], and Fukui et al. [15]. In Komori et al. [13], the authors considered a PRB turbulent flow in an open channel and observed that buoyancy driven motions cause substantial changes to the turbulence structures. Intermittent downward motions of the cold eddies with large negative peaks of temperature fluctuations are produced and contribute strongly to the turbulent transport of heat in the vertical direction. For large temperature gradients, upward and downward motions are enhanced; in this situation, not only the large-scale eddies but also small scale eddies are affected by the buoyancy-driven motion. Similar conclusions were drawn by Fukui et al. [15] analyzing the PRB turbulent flow in a duct. They noted that the turbulence structure in PRB flows was different from that observed in forced convection and argued that thermal plumes (eruptions of hot/cold fluid from the wall) induced by buoyancy became the main contributor to the production of turbulence. After Komori et al. [13], Fukui and Nakajima [14] considered a fully developed PRB turbulent flow between horizontal parallel

[1]Also at Department of Fluid Mechanics, CISM, Udine 33100, Italy.

Contributed by the Heat Transfer Division of ASME for publication in the Journal of Heat Transfer. Manuscript received January 22, 2013; final manuscript received July 10, 2013; published online November 7, 2013. Assoc. Editor: James A. Liburdy.

  

plates. They measured turbulence fluctuations and found that, with increasing temperature gradients, typical wall turbulence phenomena changed, with intensification of ejection and increase of the bursting frequency.

Numerical investigations of turbulent flow with buoyancy effects in a channel bounded by plane walls are comparatively fewer. Domaradzki and Metcalfe [16] used DNS under OB approximation to study the interaction between shear and buoyancy for thermal convection in plane Couette flow. Compared to the case of thermal convection without shear (at the same Grashof number), heat transfer may be enhanced (for $\mathrm{Gr} < 5 \times 10^4$), or reduced ($\mathrm{Gr} \simeq 1.5 \times 10^5$). For small Gr, shear acts to organize the flow into quasi-two-dimensional rolls, producing higher heat transfer rates compared to a less organized flow; for larger Gr, shear hinders plumes formation (and decreases the level of organization), and induces lower heat transfer rates. This situation may be described with a flow model in which large-scale structures are alternately driven by buoyancy or inertial effects. DNS of PRB turbulent channel flow was performed by Iida and Kasagi [17] under OB approximation. In Iida and Kasagi [17], the authors observed that thermal plumes raising from the near-wall region influence the transport mechanisms of momentum and heat through velocity-pressure gradient correlation and turbulent diffusion terms. Thermal plumes, which are spatially aligned in the streamwise direction, are also important for the dynamics of vertical structures: vertical motions of thermal plumes act to push together streamwise vortices (and associated low-speed streaks) in regions where plumes detach and rise. Recently, Zainali and Lessani [18] employed large eddy simulation to study the behavior of PRB turbulent channel flow under NOB conditions and using a low Mach number approximation to account for fluid density variations. They run simulations for different wall temperature ratios (from 1.01 to 6). Increasing the temperature gradient enhances the amount of mixing and the transport of momentum and heat (as well as fluid velocity fluctuations).

The aim of this work is to evaluate the effect of the common OB approximation in turbulent PRB flows via a campaign of DNS. We consider a channel flow of water under constant temperature gradient and assuming temperature-dependent fluid viscosity ($\mu$) and thermal expansion coefficient ($\beta$). DNS are performed at reference Reynolds, Prandtl and Richardson number using a pseudo-spectral method for the solution of a variable-properties formulation of momentum and energy equations. Simulations are run at Grashof number $\mathrm{Gr} = 1.12 \times 10^7$ and Prandtl number $\mathrm{Pr} = 3$ examining three different absolute values of the Richardson number, $\mathrm{Ri}_\tau = 926$, $\mathrm{Ri}_\tau = 498$, and $\mathrm{Ri}_\tau = 346$ (corresponding to shear Reynolds numbers $\mathrm{Re}_\tau = 110$, $\mathrm{Re}_\tau = 150$, and $\mathrm{Re}_\tau = 180$). This paper is organized as follows. The physical problem and the numerical methodology are discussed in Sec. 2. In Sec. 3, we present results of our numerical simulations. Momentum and heat transfer rates are analyzed in Sec. 3.1, whereas large scale convection in PRB turbulent flows is discussed in Secs. 3.2 and 3.3. In Sec. 3.4, we introduce a phenomenological model for heat transfer prediction in PRB flows. Flow field statistics and mixing efficiency are presented in Secs. 3.5 and 3.6. In Sec. 4, the conclusions are drawn.

## 2 Numerical Simulation of Mixed Convection in a Duct

**2.1 Physical Problem and Governing Equations.** Governing equations and numerical methodology are briefly reviewed to make the paper self-contained (further details can be found in Zonta et al. [19]). We consider an incompressible and Newtonian turbulent channel flow of water (driven by an imposed pressure gradient) with differentially-heated walls (streamwise, spanwise, and wall-normal coordinates are indicated by $x$, $y$, and $z$, respectively). A sketch of the computational domain/flow conditions is presented in Fig. 1. The size of the computational domain is

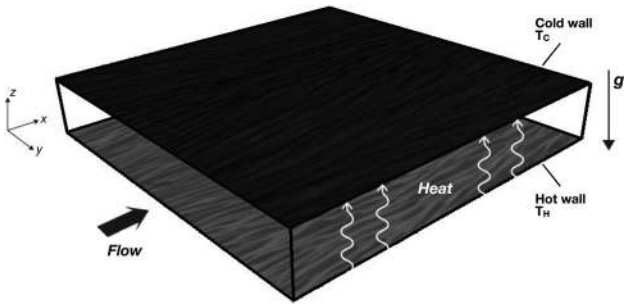


**Fig. 1 Sketch of the computational domain and flow conditions. The flow is driven along the horizontal direction ($x$) by an imposed pressure gradient. The bottom wall is kept at uniform higher temperature ($T_H$) whereas the top wall is kept at uniform lower temperature ($T_C$).**

$L_x \times L_y \times L_z = 4\pi h \times 4\pi h \times 2h$ (in $x$, $y$, and $z$, respectively), where $h$ is the half-channel height. In the present configuration, the bottom wall is kept at uniform high temperature ($T_{\mathrm{bottom}} = T_H$), whereas the top wall is kept at uniform low temperature ($T_{\mathrm{top}} = T_C$). As a consequence, the temperature difference $\Delta T_{HC} = (T_H - T_C)$ between the bottom and the top wall induces buoyancy effects within the flow field (the acceleration due to gravity acts downward along $z$). Mass, momentum, and energy balance equations for the fluid are (in dimensional form)

$$\frac{\partial u_i}{\partial x_i} = 0 \tag{1}$$

$$\rho \frac{\partial u_i}{\partial t} = -\rho u_j \frac{\partial u_i}{\partial x_j} + \frac{\partial}{\partial x_j}\left(\mu \frac{\partial u_i}{\partial x_j}\right) - \frac{\partial p}{\partial x_i} + (\rho - \rho_{\mathrm{ref}}) g_i + \delta_{1,i} \tag{2}$$

$$\rho c_p \frac{\partial T}{\partial t} + \rho c_p u_j \frac{\partial T}{\partial x_j} = \frac{\partial}{\partial x_j}\left(\lambda \frac{\partial T}{\partial x_j}\right) \tag{3}$$

where $u_i$ is the $i$th component of the velocity vector, $g_i$ is the $i$th component of the gravitational acceleration vector, $p$ is the fluctuating kinematic pressure, $\delta_{1,i}$ is the mean pressure gradient that drives the flow, $T$ is temperature, $\rho$ is density, $\mu$ is viscosity, $\lambda$ is thermal conductivity, and $c_p$ is specific heat. Three different dimensionless numbers are defined: the Reynolds number $\mathrm{Re}_\tau = (u_\tau h/\nu_{\mathrm{ref}})$, the Prandtl number $\mathrm{Pr} = (\mu_{\mathrm{ref}} c_{p,\mathrm{ref}})/(\lambda_{\mathrm{ref}})$ and the Grashof number $\mathrm{Gr} = (g\beta_{\mathrm{ref}} \Delta T_{HC} (2h)^3)/(\nu_{\mathrm{ref}}^2)$, where the subscript ref is used to indicate fluid properties at the reference temperature $T_{\mathrm{ref}} = (T_H + T_C)/2$ and $u_\tau$ is the shear velocity. Note that $\beta_{\mathrm{ref}} = -(1/\rho)(\partial\rho/\partial T)_p$ and $\nu_{\mathrm{ref}} = (\mu_{\mathrm{ref}}/\rho_{\mathrm{ref}})$ are the thermal expansion coefficient and the kinematic viscosity at the reference temperature. For PRB turbulent flows, the key parameter is the Richardson number Ri (which measures the importance of buoyancy compared to inertia). Here, we used the absolute value of the shear Richardson number $\mathrm{Ri}_\tau = |\mathrm{Gr}/\mathrm{Re}_\tau^2|$ (for convectively unstable flows, the Richardson number is negative). Within the framework of this study, we consider all the fluid properties uniform but $\mu$ and $\beta$ [4,20]. Note that the incompressibility hypothesis is perfectly sound within the framework of our numerical method, since $\Delta\rho/\rho < 2\%$ for the range of parameters analyzed in this study. The resulting set of equations is discretized using a pseudo-spectral method based on transforming the field variables into wavenumber space, through Fourier representations for the periodic (homogeneous) directions $x$ and $y$, and Chebychev representation for the wall-normal (nonhomogeneous) direction $z$ (see Refs. [19,20] for details).

**2.2 Summary of the Simulations.** For the present flow configuration of PRB turbulent channel flow (sketched in Fig. 1), we performed an extensive campaign of numerical simulations (see Table 1). The size of the computational domain ($4\pi h \times 4\pi h \times 2h$)

**Table 1 PRB turbulent channel flow: summary of the simulations parameters. Simulations for the reference case of forced convection turbulence (FC) are also included.**

| Simulations | $Re_\tau$ | $Ri_\tau$ | Grid | Thermophysical properties | |
|---|---|---|---|---|---|
| *PRB*110 − *Boussinesq* | 110 | 926 | $256 \times 512 \times 257$ | Uniform | PRB |
| *PRB*110 − $\mu(T)$ | 110 | 926 | $256 \times 512 \times 257$ | $\mu = \mu(T)$ | Flow |
| *PRB*110 − $\beta(T)$ | 110 | 926 | $256 \times 512 \times 257$ | $\beta = \beta(T)$ | |
| *PRB*150 − *Boussinesq* | 150 | 498 | $256 \times 512 \times 257$ | Uniform | |
| *PRB*150 − $\mu(T)$ | 150 | 498 | $256 \times 512 \times 257$ | $\mu = \mu(T)$ | |
| *PRB*150 − $\beta(T)$ | 150 | 498 | $256 \times 512 \times 257$ | $\beta = \beta(T)$ | |
| *PRB*180 − *Boussinesq* | 180 | 346 | $256 \times 512 \times 257$ | Uniform | |
| *PRB*180 − $\mu(T)$ | 180 | 346 | $256 \times 512 \times 257$ | $\mu = \mu(T)$ | |
| *PRB*180 − $\beta(T)$ | 180 | 346 | $256 \times 512 \times 257$ | $\beta = \beta(T)$ | |
| *FC*110 | 110 | 0 | $256 \times 256 \times 257$ | Uniform | Forced |
| *FC*150 | 150 | 0 | $256 \times 256 \times 257$ | Uniform | Convection |
| *FC*180 | 180 | 0 | $256 \times 256 \times 257$ | Uniform | |

and the grid resolution ($256 \times 512 \times 257$ grid points) for each simulation were chosen to resolve explicitly the largest and the smallest flow scales [21] (requirements imposed by DNS). For the range of parameters chosen in this study ($Gr \simeq 10^7, Re_\tau < 200$), we used a very refined grid [16–18,21,22]. The size of the computational domain employed for present DNS is larger compared to archival literature. The only exceptions are some test simulations done by Iida and Kasagi [17] on an elongated (but narrow) channel ($7.5\pi h \times 3\pi h \times 2h$). As a consequence, present simulations require huge computational resources (500,000 h central processing unit (CPU) time) and represent the state of the art in the field of turbulent PRB flows. We performed three different types of simulations:

(1) base simulations with uniform thermophysical properties (OB approximation), referred to as *Boussinesq*
(2) simulations where fluid viscosity changes according to the relation $\mu(T) = A \times 10^{B/(T-C)}$ [4,19], where $T$ is the local fluid temperature in Kelvin, while $A = 2.414 \times 10^{-5}$, $B = 247.8$, and $C = 140$. These simulations will be referred to as $\mu(T)$
(3) simulations where fluid thermal expansion coefficient changes as $\beta(\theta^-) = \beta_{ref}(1 + 0.29 \times (\theta^-) - 0.037 \times (\theta^-)^2)$ [4,20], where $\theta^- = (T - T_{ref})/(\Delta T_{HC}/2)$ is the dimensionless temperature. These simulations will be referred to as $\beta(T)$

A temperature difference $\Delta T_{HC} = T_H - T_C = 40$K is imposed between the hot and the cold wall, which are kept at $T_H = 343$ K and $T_C = 303$ K, respectively. All simulations are performed at reference Prandtl number $Pr = 3$ and Grashof number $Gr = 1.12 \times 10^7$. Note that $Pr \simeq 3$ is the Prandtl number of water at the reference temperature $T_{ref} = 323$ K. Three different reference shear Reynolds number are considered in this study: $Re_\tau = 110$, $Re_\tau = 150$, and $Re_\tau = 180$. As a consequence, computations are run at three different absolute values of the shear Richardson number, $Ri_\tau = |Gr/Re_\tau^2|$: $Ri_\tau = 926$ ($Re_\tau = 110$), $Ri_\tau = 498$ ($Re_\tau = 150$), and $Ri_\tau = 346$ ($Re_\tau = 180$). A comprehensive overview of the simulations parameters is provided in Table 1.

## 3 Results and Discussion

**3.1 Wall-Normal Momentum and Heat Transfer Efficiency.** To establish whether local flow modifications due to NOB effects have an impact on macroscopic parameters of PRB turbulent channel flow we compute the friction factor ($C_f$) and the bulk Nusselt number ($Nu_b$) as

$$C_f = \frac{\tau_w}{\frac{1}{2}\rho u_b^2}, \quad Nu_b = \frac{q_w D_h}{\lambda(T_W - T_b)} \tag{4}$$

where $\tau_w = \mu \partial\langle u\rangle/\partial z$ is the viscous shear stress at the wall, $q_w = \lambda \partial\langle T\rangle/\partial z$ is the diffusive heat flux at the wall, $u_b = \frac{1}{A}\int_A \langle u\rangle dA$ is the bulk velocity, and $T_b = \int_A \langle T\rangle\langle u\rangle dA / \int_A \langle u\rangle dA$ is the bulk temperature (A being a cross section of the channel). Brackets indicate average in time and in space (over the homogeneous directions). Note that the bulk Reynolds number may be defined as $Re_b = \rho u_b D_h/\mu$, where $D_h = 4h$ is the hydraulic diameter. We will also consider the centerline Nusselt number, $Nu_c = q_w h/(\lambda(T_W - T_{ref}))$, where $T_W = \Delta T_{HC}/2$ is the wall-temperature made symmetrical with respect to the reference temperature. Measurements of the Nusselt numbers ($Nu_b$ and $Nu_c$) and of the friction factor ($C_f$) for the case of turbulent forced convection have been performed to obtain reference benchmark data (useful for comparison purposes, see Table 2). Note that for

**Table 2 Friction factor ($C_f$) and Nusselt numbers ($Nu_b$, $Nu_c$) for the case of forced convection turbulence. Simulations for $Re_\tau = 110$ are performed on a grid made of $128 \times 128 \times 129$ nodes. Simulations from $Re_\tau = 150$ and $Re_\tau = 180$ are performed on a grid made of $256 \times 256 \times 257$ nodes. When $\mu = \mu(T)$ friction factors $C_f^H$ and $C_f^C$ are evaluated at the hot and cold wall, respectively. Reference data from currently available correlations are also provided: we use [23] $C_f = 0.073 \times Re_m^{-1/4}$ (label DE) and [24] $Nu_b = 0.027 \times Re_b^{4/5} Pr^{1/3}$ (label ST). Note that $Re_m = Re_b/2$.**

| Simulations | $Re_\tau$ | $Ri_\tau$ | $Re_b$ | $C_f$ ($\times 10^{-3}$) | | $C_f$ (DE) ($\times 10^{-3}$) | $Nu_b$ | $Nu_b$ (ST) | $Nu_c$ |
|---|---|---|---|---|---|---|---|---|---|
| | | | | $C_f^C$ | $C_f^H$ | | | | |
| *FC*110 − *uniform* | 110 | 0 | 6445 | 9.3 | | 9.7 | 37.5 | 43.4 | 8.1 |
| *FC*110 − $\mu = \mu(T)$ | 110 | 0 | 6371 | 10.8 | 8.2 | 9.7 | 37.5 | 43 | 8.1 |
| *FC*150 − *uniform* | 150 | 0 | 9198 | 8.5 | | 8.9 | 52 | 57.7 | 11.3 |
| *FC*150 − $\mu = \mu(T)$ | 150 | 0 | 9113 | 10.1 | 7.7 | 8.9 | 52.1 | 57.3 | 11.4 |
| *FC*180 − *uniform* | 180 | 0 | 11269 | 8.2 | | 8.4 | 63.1 | 67.9 | 13.6 |
| *FC*180 − $\mu = \mu(T)$ | 180 | 0 | 11085 | 9.4 | 7.4 | 8.4 | 63 | 67.1 | 13.6 |

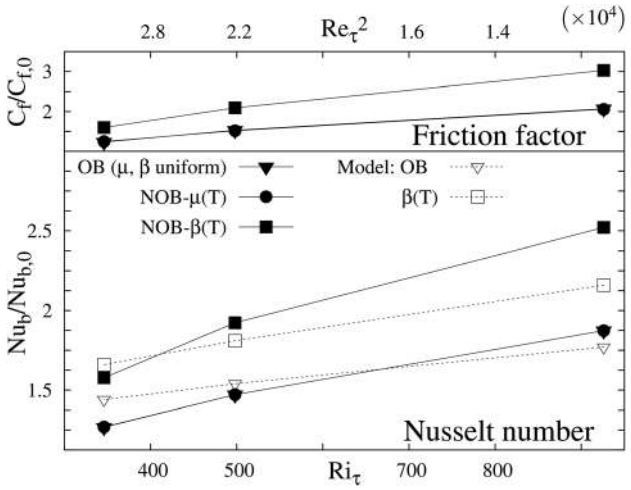


**Fig. 2 (*a*) Normalized friction factor ($C_f/C_{f,0}$) and Nusselt number ($Nu_b/Nu_{b,0}$) for simulations of PRB turbulent channel flow: –▼– represents results obtained with OB assumptions; –●– represents results obtained assuming $\mu(T)$; –■– represents results obtained assuming $\beta(T)$. Results of $Nu_b/Nu_{b,0}$ obtained from our simplified model of heat transfer in PRB flows (open symbols) are also shown: –∇– for OB assumptions, –□– for $\beta(T)$.**

turbulent forced convection only $\mu(T)$ is considered (no buoyancy effects, hence $\beta(T)$ is negligible). It is clear that even for this reference case, $\mu(T)$ has an important effect: the local value of the friction factor computed at the cold ($C_{f,C}$) and hot wall ($C_{f,H}$) is different (±15%) from the value computed assuming uniform fluid properties. These differences are due to the different values of the shear stress at the wall ($\tau_w = \mu\partial\langle u\rangle/\partial z$), which in turns depends on the local value of the fluid viscosity. By contrast, the Nusselt number is not influenced by $\mu(T)$. This happens in this specific flow configuration, where the total heat flux is constant across the channel. In Table 2, we also provide reference data for $C_f$ and $Nu_b$ obtained from currently available correlations. In particular, we use $C_f = 0.073 \times Re_m^{-1/4}$ [23] and $Nu_b = 0.027 \times Re_b^{4/5} Pr^{1/3}$ [24]. Note that $Re_m = Re_b/2$.

Measurements of Nusselt numbers ($Nu_b$ and $Nu_c$) and friction factor ($C_f$) for the case of PRB turbulent channel flow are shown in Fig. 2 and summarized in Table 3. Compared to the reference case of turbulent forced convection ($C_{f,0}$ and $Nu_{b,0}$) the friction factor $C_f$ and the Nusselt number $Nu_b$ for PRB turbulent channel flow with uniform fluid properties (OB approximation, –▼– in Fig. 2) increases monotonically in the $Ri_\tau$ parameter space ($1.2 < C_f/C_{f,0} < 2$ and $1.3 < Nu_b/Nu_{b,0} < 1.9$). The role of $\beta(T)$ (–■– in Fig. 2) is important, whereas the role of $\mu(T)$ is negligible (–●– in Fig. 2(*a*)): compared to the OB approximation (–▼– in Fig. 2), when $\beta(T)$ is considered $C_f$ and $Nu_b$ increase up to +40% (for $Ri_\tau = 926$). An explanation of these results, based on the analysis of turbulence structures/statistics, will be given in the following sections. Here, we just mention that the turbulence structure of PRB flow is essentially different from that of forced convection: for PRB flows, rising, and falling thermal plumes (generated by buoyancy at the hot and cold walls) induce a large scale thermal convection, which is responsible for the increase of momentum and heat transport efficiency (these mechanisms have no counterparts in forced convection turbulence). In Sec. 3.4, we will compare our numerical results with a phenomenological model for heat transfer prediction in PRB turbulent flows.

**3.2 Large Scale Convection.** In Sec. 3.1, we have analyzed the effect of NOB on heat and momentum transfer coefficients in PRB turbulent flows. In this section, we try to link those results

**Table 3 Friction factor ($C_f$) and Nusselt numbers ($Nu_b$, $Nu_c$) for PRB turbulent channel flow. When $\mu = \mu(T)$ friction factors $C_f^H$ and $C_f^C$ are evaluated at the hot and cold wall, respectively.**

| Simulations | $Re_\tau$ | $Ri_\tau$ | $Re_b$ | $C_f$ $C_f^C$ | $C_f$ $C_f^H$ | $(\times 10^{-3})$ | $Nu_b$ | $Nu_c$ |
|---|---|---|---|---|---|---|---|---|
| *PRB*110 – *Boussinesq* | 110 | 926 | 4230 | 18.6 | | | 71 | 18.4 |
| *PRB*110 – $\mu(T)$ | 110 | 926 | 4230 | 19.6 | 17.4 | | 71 | 18.2 |
| *PRB*110 – $\beta(T)$ | 110 | 926 | 3555 | 28 | | | 94 | 25.2 |
| *PRB*150 – *Boussinesq* | 150 | 498 | 7470 | 13 | | | 76.5 | 18.8 |
| *PRB*150 – $\mu(T)$ | 150 | 498 | 7220 | 12.1 | 13.6 | | 76.5 | 18.7 |
| *PRB*150 – $\beta(T)$ | 110 | 498 | 6320 | 17.8 | | | 100 | 24.3 |
| *PRB*180 – *Boussinesq* | 180 | 346 | 10040 | 10.1 | | | 80 | 19.6 |
| *PRB*180 – $\mu(T)$ | 180 | 346 | 9707 | 9.4 | 10.9 | | 80.1 | 19.5 |
| *PRB*180 – $\beta(T)$ | 110 | 346 | 8820 | 13.1 | | | 99.5 | 24.1 |

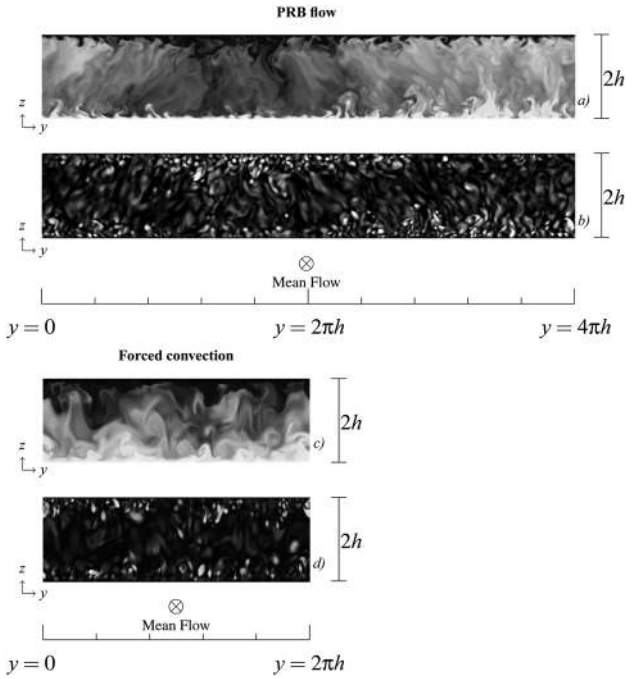


**Fig. 3 Contour maps of the temperature field (panels a and c) and of the streamline rotation vector (panels b and d) on a $x - y$ plane parallel to the walls (and passing through the centerline of the channel) for simulations of channel turbulence at $Re_\tau = 150$. (*a*) PRB turbulent channel flow ($Ri_\tau = 498$). (*b*) Forced convection turbulence.**

with the dynamics of flow structures. In Fig. 3, flow structures are analyzed using contour maps of the temperature field (panels *a* and *c*) and of the streamline rotation vector Ω [25] (panels *b* and *d*). Figs. 3(*a*) and 3(*b*) refer to PRB flow, Figs. 3(*c*) and 3(*d*) to forced convection. Note that Figs. 3(*a*) and 3(*b*) refer to a domain twice as large as that of Figs. 3(*c*) and 3(*d*). In the reference case of forced convection turbulence, quasi-streamwise vortices (light regions in Fig. 3(*d*)) are the dominant flow structures [26]. Temperature (Fig. 3(*c*)) is advected by the velocity field, and is transported by vertical motions: a thick layer of hot fluid (resp. cold fluid) is observed near the hot wall (resp. cold wall). In PRB flows, the turbulence structure is essentially different from that of forced convection. We will take Fig. 3(*a*) as reference to provide physical explanations of the transport mechanisms in PRB turbulent channel flows. The most unstable regions of the flow are those close to the boundaries (where large temperature gradients exist),

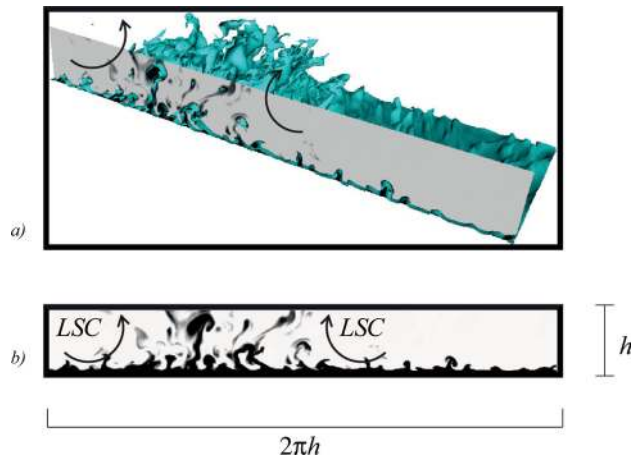


**Fig. 4 (*a*) Flow structures for PRB turbulent channel flow: structures are plotted on a specific region of the fluid domain using a dimensionless temperature isosurface ($\theta = 0.16$). (*b*) The trace of temperature isosurface on a cross section (temperature contour) is shown to clarify the mechanisms of formation and merging of buoyant plumes. LSC: large scale circulation.**

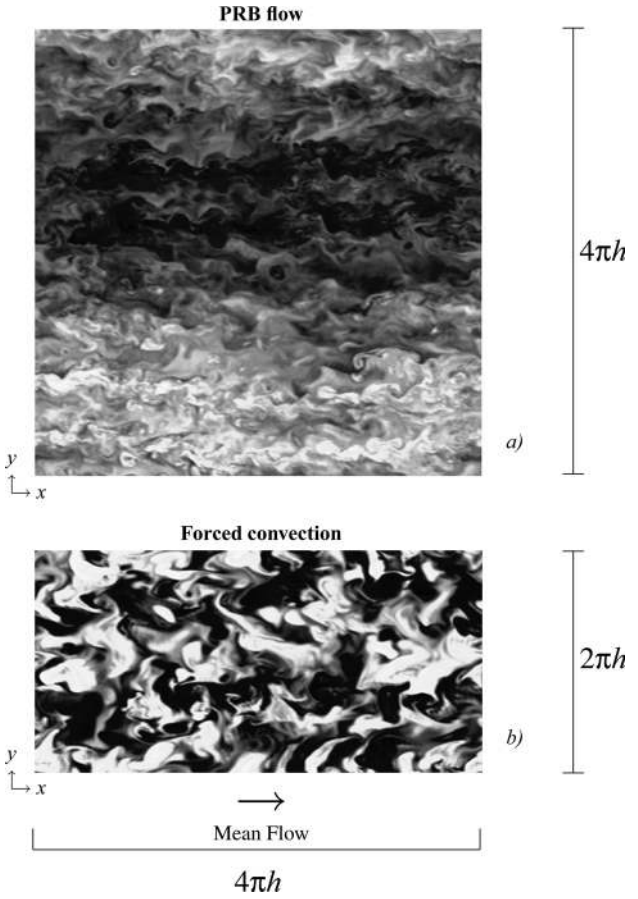


**Fig. 5 Contour maps of the temperature field on a $x - y$ plane parallel to the walls (and passing through the centerline of the channel) for simulations of channel turbulence at $Re_\tau = 150$. (*a*) PRB turbulent channel flow ($Ri_\tau = 498$). (*b*) Forced convection turbulence.**

and the dominant feature of the flow (large eddies) originate there. Consider the hot (bottom) wall: there are intermittent eruptions of hot fluid away from this wall (light regions in Fig. 3(*a*)). Colder fluid moves close to the hot wall (dark regions in Fig. 3(*a*)) to replace the fluid in an eruption. This is gradually heated by conduction from the wall until there is a thick enough layer of hot fluid for another eruption to be originated. The process then repeats. Each eruption gives rise to one or sometimes more columns of hot fluid rising through the interior region. These features are called *thermals plumes*, or simply *thermals* [27]. They penetrate right across the layer generating transient "bubbles" of fluid close to the opposite boundary. Near the lower wall the upward velocity of a rising hot plume is initially low. In the core region, it is accelerated by buoyancy forces and eventually penetrates the boundary layer at the upper wall with high kinetic energy. Thermals lose their identity before reaching the opposite boundary, where they are deflected in the horizontal direction. The deflection of thermals generates a strong divergence of the horizontal velocity field in the boundary layer, which pushes newly forming plumes closer yet producing the large scale convection [22]. The mechanisms of formation/merging of buoyant plumes is visualized in Fig. 4: plumes appear first as instabilities in the thermal boundary layer; later, plumes cluster together to form a large-scale structure whose characteristic dimension scales with the height of the channel. We note a tendency for several successive eruptions to occur with periodicity and in the same places each time. Thermals formation and persistence appears to be one of the dominant feature of buoyancy-affected flows [10]. The quasi streamwise vortices (light regions in Fig. 3(*b*)) seem to be swept out by the large scale circulation induced by thermal plumes. Coherent, large scale motions induced by thermals and disorganized small-scale motions coexist, the latter occurring both within the thermals and in the region between adjacent thermals (light regions in Fig. 3(*b*)). Thermal plumes are aligned in the streamwise direction due to the mean shear. This is visualized through temperature contours on a $x - y$ plane passing through the centerline of the channel (Fig. 5). Note that the domain in Fig. 5(*a*) is twice as large as that of Fig. 5(*b*), as discussed before. For PRB turbulent channel flow (Fig. 5(*a*)), we observed two different regions: a region of hot fluid (light region), corresponding to thermal plumes raising from the hot wall, and a region of cold fluid (dark region), corresponding to thermal plumes falling down from the cold wall. Temperature contours for the reference case of forced convection turbulence (Fig. 5(*b*)) is shown for comparison purposes. In this case, large scale circulation does not occur, and regions of hot (light regions) and cold fluid (dark regions) are homogeneously distributed.

**3.3 Frequency Spectra.** So far, we have observed that PRB turbulent channel flow is characterized by flow structures of different scales: from individual convective plumes (scaling with the boundary layer thickness) to large scale clusters of plumes (scaling with the height of the computational domain). To quantify the distribution of energy to the different scales, we measured the spanwise energy spectra [17] of the streamwise velocity fluctuations ($E_{u_x^2}$, Fig. 6(*a*)), of the spanwise velocity fluctuations ($E_{u_y^2}$, Fig. 6(*b*)) and of the wall-normal velocity fluctuations ($E_{u_z^2}$, Fig. 6(*c*)). For each component, we compared results from the simulation assuming OB approximation (filled circles) with those assuming NOB conditions ($\beta(T)$, open circles). Results from simulation of forced convection turbulence (*solid line*) are also shown for comparison purposes. Since the effect of $\mu(T)$ is low compared to that of $\beta(T)$, here, we discuss only $\beta(T)$ as temperature-dependent fluid property. Frequency spectra, computed at the channel center ($L_x/2$, $L_z/2$), are averaged over a time window of $\Delta t^+ = \Delta t \cdot u_\tau/\nu = 1 \times 10^4$ after a statistically steady state is reached. Results are shown for simulations at $Ri_\tau = 498$ ($Re_\tau = 150$) only. For frequency spectra in PRB turbulent channel flow with OB approximation (filled circles) we observed (i) a general increase of energy spectra at higher wave numbers, corresponding to higher small scale mixing (note the small scale structures in Figs. 3(*a*), 3(*b*), and 5(*a*)), (ii) a general decrease of

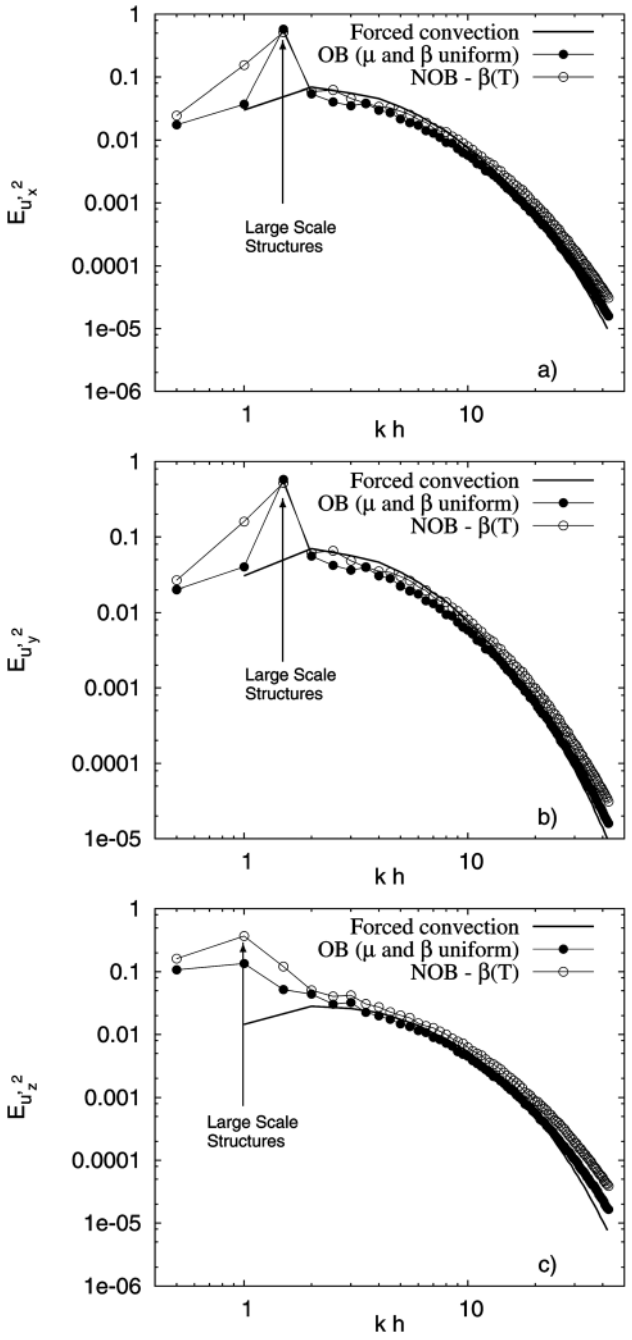


**Fig. 6 Spanwise frequency spectra of fluid velocity fluctuations ($Ri_\tau = 498$) for PRB turbulent channel flow: comparison between simulations with uniform thermophysical properties (filled circles) and simulations with temperature-dependent thermal expansion coefficient (open circles). Results from the simulation of forced convection turbulence (solid line) are also included. (*a*) Streamwise velocity fluctuations; (*b*) spanwise velocity fluctuations; (*c*) wall-normal velocity fluctuations.**

energy spectra at moderate wave numbers, and (iii) a peak value at low wave numbers, which has no counterpart in the corresponding turbulent forced convection (lines). Decrease of frequency spectra at moderate wave numbers (which include the streak spacing) indicates the attenuation of mechanism of generating and sustaining the typical coherent structures observed in usual channel turbulence [17]. Increase of energy spectra at low wave numbers is due to large scale convection prompted by thermal plumes emerging from the near wall region (see Sec. 3.2). To demonstrate this correlation, we consider a large scale structure of length scale $h$ and velocity scale $u_{LS}$ (and frequency $f_{LS}$): the scale velocity $u_{LS} = \sqrt{g\beta\Delta T_{HC} 2h} = \sqrt{\mathrm{Gr}}\nu/2h$ is the free-fall velocity [5], whereas the corresponding frequency is $f_{LS} = u_{LS}/2\pi h = 0.6$ Hz. From Fig. 6, we observe that the peak values of the frequency spectra occur for $kh \simeq 1$. The frequency associated to this wavenumber is $f = ku_{LS}/2\pi = 0.63$ Hz, in good agreement with the previous estimate. The effect of $\beta(T)$ is marked throughout the entire range of wavenumbers. In particular, we observe that $\beta(T)$ increases the energy of turbulence fluctuations at each lengthscale, indicating that energy is introduced at larger as well as smaller lengthscales. Interestingly, the peak value of the spanwise energy spectra is not influenced by $\beta(T)$, meaning that large scale structures are controlled by the size of the domain ($h$) rather than by the local value of $\beta(T)$. Modifications of large and small-scale eddies have an impact on wall-normal transport of momentum and heat (Sec. 3.1) and are expected to influence mixing properties of the flow (see Sec. 3.6).

**3.4 A Phenomenological Model of Heat Transfer in PRB Turbulent Flows.** In this section, we propose a simplified model of heat transfer in PRB turbulent flows. We build our model following that of Hetsroni et al., [28] which was developed for heat transfer prediction in buoyancy-free (forced convection) turbulent flows. Some of the details derived in Hetsroni et al. [28] have been included here for completeness. We assume that the amount of heat $Q$ removed from the wall during the time $t$ is determined primarily by the coherent flow structures: bursting events and thermal plumes (see Sec. 3.2 for details on coherent structures in PRB flows). This is a fair assumption for turbulent flows influenced by buoyancy [28]. A coherent structure (burst/plume) is modeled as an axially symmetrical submerged jet. The heat transferred from the wall by a submerged jet of cross-sectional area $s$ and duration $t_1$ is [28] $Q_1 = 2\rho c_p w_m \Delta T_m s t_1 I$, where $I \simeq A/\mathrm{Pr}^n$ (for water, $A = 0.0667$ and $n = 0.8$), $w_m$ and $T_m$ are the velocity and the temperature at the axis of the jet while $\Delta T_m = T_m - T_{\mathrm{ref}}$ ($T_{\mathrm{ref}}$ is the centerline reference temperature). Within the present model, the characteristic velocity of the jet is the sum of two vertical velocities: one is the characteristic velocity of a burst ($w_{m,\mathrm{burst}}$) while the other is the characteristic velocity of a plume ($w_{m,\mathrm{plume}}$). Since the total amount of heat removed from the wall is $Q = \alpha(T_w - T_{\mathrm{ref}})$, the thermal balance reads as

$$Q = \alpha(T_w - T_{\mathrm{ref}}) = 2\rho c_p (w_{m,\mathrm{burst}} + w_{m,\mathrm{plume}})\Delta T_m \gamma (A/\mathrm{Pr}^n) \quad (5)$$

with $\alpha$ the heat transfer coefficient and $\gamma = t_1/t$. In dimensionless form (multiplying by $h/\lambda(T_w - T_{\mathrm{ref}})$ and assuming $\Delta T_m = T_w - T_{\mathrm{ref}}$), Eq. (5) becomes

$$\mathrm{Nu}_b = \underbrace{2\frac{\mu}{\nu}c_p w_m \gamma \frac{A}{\mathrm{Pr}^n}\frac{h}{\lambda}}_{\mathrm{Nu}_{b,0}} + \underbrace{2\frac{\mu}{\nu}c_p w_{m,\mathrm{plume}} \gamma \frac{A}{\mathrm{Pr}^n}\frac{h}{\lambda}}_{\mathrm{Nu}_{b,t}} \quad (6)$$

where $\mathrm{Nu}_b = \alpha h/\lambda$. Note that the Nusselt number may be considered as the sum of a contribution due to turbulent bursts ($\mathrm{Nu}_{b,0}$, buoyancy is neglected) and a contribution due to thermal plumes ($\mathrm{Nu}_{b,t}$). Eq. 6 may be written as $\mathrm{Nu}_b/\mathrm{Nu}_{b,0} = 1 + w_{m,\mathrm{burst}}/w_{m,\mathrm{plume}}$, where $w_{m,\mathrm{burst}} = \varepsilon u_b$ (with $u_b$ is the bulk velocity) and $w_{m,\mathrm{plume}} = (g\beta_{\mathrm{ref}}\Delta T_{HC} 2h)^{1/2} = 1/2\mathrm{Gr}^{1/2}\nu/h$ (namely, the free-fall velocity [5]). Since bursts originated in the near-wall region expand into the outer region with a wall-normal velocity comparable with the streamwise convection velocity, we assume $w_{m,\mathrm{burst}} \simeq u_b$, and hence $\varepsilon \simeq 1$. For wall-bounded turbulent flows, the bulk velocity may be expressed as $u_b/u_\tau = 8.74\mathrm{Re}_\tau^{1/7}$ [29]. With these assumptions, we obtain

$$\frac{\mathrm{Nu}_b}{\mathrm{Nu}_{b,0}} \simeq 1 + \frac{1}{20}\frac{\mathrm{Gr}^{1/2}}{\mathrm{Re}_\tau}\frac{1}{\mathrm{Re}_\tau^{1/7}} = 1 + \frac{1}{20}\frac{\mathrm{Ri}_\tau^{1/2}}{\mathrm{Re}_\tau^{1/7}} \quad (7)$$

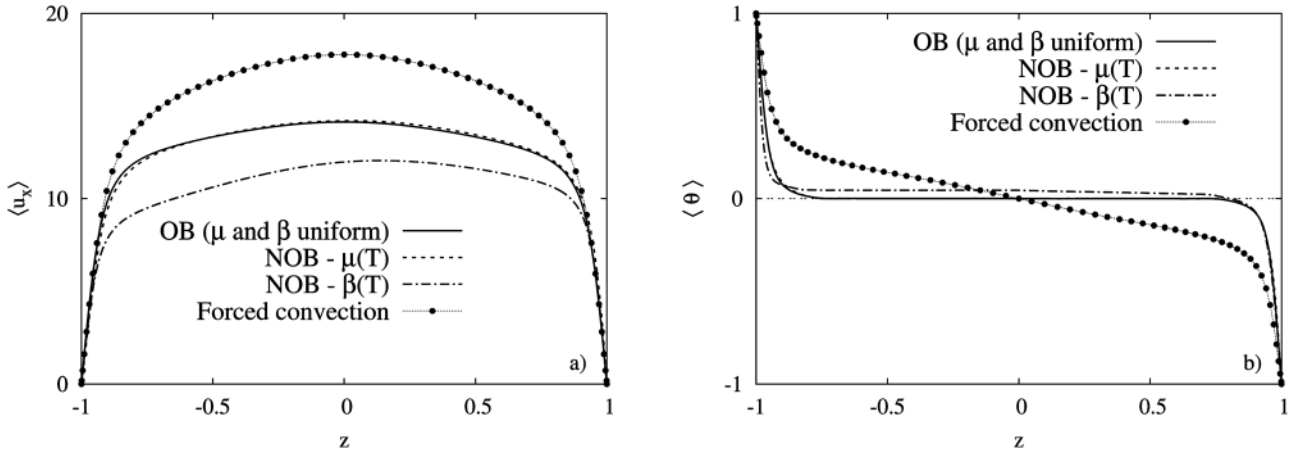


**Fig. 7 Statistics of mean fluid velocity and temperature for PRB turbulent channel flow at $Ri_\tau = 498$ ($Re_\tau = 150$): comparison between simulations with uniform thermophysical properties (OB, solid line) and simulations with temperature-dependent viscosity (NOB, dashed line) and temperature-dependent thermal expansion coefficient (NOB, dash-dotted line). Results from the simulation of forced convection turbulence (symbols) are also included. (*a*) Mean fluid streamwise velocity $\langle u_x \rangle$; (*b*) mean fluid temperature $\langle \theta \rangle$.**

For our simulations, $Nu_b/Nu_{b,0} \simeq 1.44$ (for $Ri_\tau = 346$ and $Re_\tau = 180$), $Nu_b/Nu_{b,0} \simeq 1.54$ (for $Ri_\tau = 498$ and $Re_\tau = 150$), and $Nu_b/Nu_{b,0} \simeq 1.77$ (for $Ri_\tau = 926$ and $Re_\tau = 110$). When $\beta(T)$ is considered, the characteristic velocity of the plume should be corrected to represent the vertical velocity of a jet in a fluid with non uniform $\beta$. Assuming $w^{NOB}_{m,plume} = (\beta_{bulk}/\beta_{ref}) w_{m,plume}$ and $\beta_{bulk}$ the bulk thermal expansion coefficient, we obtain

$$\frac{Nu_b}{Nu_{b,0}} \simeq 1 + \left(\frac{\beta_{bulk}}{\beta_{ref}}\right)^{1/2} \frac{1}{20} \frac{Ri_\tau^{1/2}}{Re_\tau^{1/7}} \tag{8}$$

In our simulations $(\beta_{bulk}/\beta_{ref})^{1/2} = 1.505$, leading to: $Nu_b/Nu_{b,0} \simeq 1.66$ (for $Ri_\tau = 346$ and $Re_\tau = 180$), $Nu_b/Nu_{b,0} \simeq 1.81$ (for $Ri_\tau = 498$ and $Re_\tau = 150$), and $Nu_b/Nu_{b,0} \simeq 2.16$ (for $Ri_\tau = 926$ and $Re_\tau = 110$). Values of $Nu_b$ obtained from the present model for both uniform properties (open triangles, $-\nabla-$) and $\beta(T)$ (open squares, $-\square-$) are shown in Fig. 2 together with our DNS results. Note that there is a quadratic dependence between Nu and Gr, while there is an almost inverse linear dependence between Nu and Re. The phenomenological model developed here predicts the importance of NOB assumptions on heat transfer rates: differences (up to 30%) may be observed between the results obtained for OB ($-\nabla-$) and for NOB ($-\square-$) conditions. Qualitative agreement between our simplified model and DNS results is also observed, although there are some differences. In particular, this model seems to underestimate the amount of heat transported by thermal plumes in case of NOB conditions and large values of $Ri_\tau$. The problem of Nusselt number (Nu) calculation in forced convection has been extensively investigated in literature, and several numerical correlations have been developed. By contrast, numerical correlations for Nu prediction in mixed convection are scarce. When it is considered in this context, the present model is useful for prediction of heat transfer enhancement (compared to the case of forced convection) in turbulent mixed convection.

**3.5 Flow Field Statistics.** In this section, flow field statistics are analyzed and discussed, and the role of temperature-dependent fluid properties is pointed out. To keep discussion contained, statistics will be examined only for $Ri_\tau = 498$. Velocity, temperature, and the wall normal coordinate are made dimensionless as $u^+ = u/u_\tau, \theta^- = (T - T_{ref})/(\Delta T_{HC}/2)$, and $z^- = z/h$, respectively. Unless explicitly indicated, all the quantities in this section (and in the following) are expressed in dimensionless units, with the superscript + or – being suppressed for ease of notation.

In Fig. 7, the mean streamwise velocity profiles, $\langle u_x \rangle$, and the mean temperature profile, $\langle \theta \rangle$, are shown (in dimensionless units) as a function of the dimensionless wall-normal coordinate $z$. Results from simulations with uniform thermophysical properties (solid line), with temperature-dependent viscosity ($\mu(T)$, dotted line) and with temperature-dependent thermal expansion coefficient ($\beta(T)$, dash-dotted line) are compared. Profiles of $\langle u_x \rangle$ and $\langle \theta \rangle$ from the reference simulation of turbulent forced convection (symbols) are also included for comparison purposes. Due to the effect of buoyancy in PRB turbulent flows, wall-normal transport of momentum, and heat increases compared to the case of forced convection turbulence, where temperature is a passive scalar. The mean streamwise velocity for PRB turbulent flow (lines in Fig. 7(*a*)) is globally decreased, and the central part of the profile (flat) is typical of a well mixed profile. This suggests that turbulence (and the associated wall-normal transport of momentum) is much activated by buoyancy, causing the thinning of the boundary layer thickness and the increase of the skin friction (see also Sec. 3.1). From Fig. 7(*a*), we note that the NOB effects may be important. In particular, $\beta(T)$ globally decreases the mean velocity profiles compared to the simulation with OB assumption. By contrast, the effect of $\mu(T)$ is only marginal. The mean temperature field (Fig. 7(*b*)) has a two-region structure consisting of a well-mixed interior (extending over a large proportion of the channel) that separates the boundary layers at the lower and upper walls. It is clear that buoyancy effects in PRB flow (solid line) increases the temperature gradient at the wall but decreases the temperature gradient elsewhere. As a consequence, higher heat transfer rates are observed at the wall (see Sec. 3.1), whereas enhanced turbulent mixing is expected in the core of the channel. Temperature-dependent fluid properties may alter the symmetry of the fluid velocity and temperature profiles in the wall-normal direction. We note that only the effect of $\beta(T)$ is visible. The mean fluid temperature profile obtained from NOB – $\mu(T)$ simulation is barely visible, since it lies behind that obtained from OB simulation. Due to the temperature behavior of $\beta(T)$, buoyancy supports the uprising hot fluid more than the downcoming cold fluid, resulting in a slight increase of the bulk temperature. However, the flow asymmetry induced by NOB conditions is low compared to the overall effect of buoyancy (thermal convection) on PRB turbulent channel flow. For this reason, we will present the following statistics for half domain only (average has been done between the results for $-1 < z < 0$ and those for $0 < z < 1$).

We have already observed in Sec. 3.1 that the Nusselt number (Nu) and the friction factor ($C_f$) increase in PRB turbulent channel

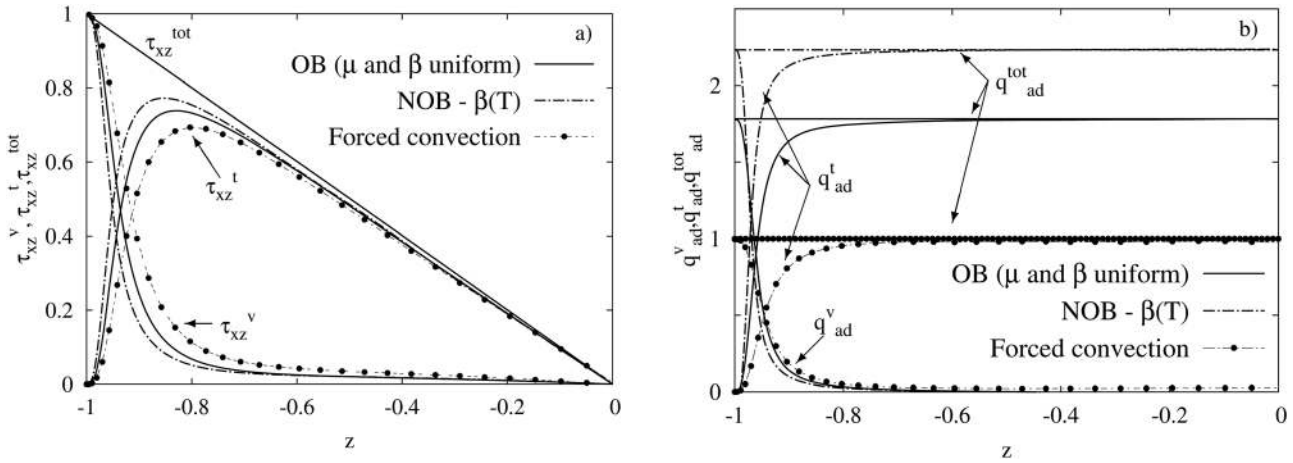


**Fig. 8 Wall-normal transport of momentum and heat for PRB turbulent channel flow at $Ri_\tau = 498$ ($Re_\tau = 150$): comparison between simulations with uniform thermophysical properties (OB, solid line) and simulation with temperature-dependent thermal expansion coefficient (NOB, dash-dotted line). Results from the simulation of forced convection turbulence (symbols) are also included. (*a*) Wall-normal behavior of the total ($\tau_{xz}^{tot}$), turbulent ($\tau_{xz}^{t}$), and viscous ($\tau_{xz}^{v}$) shear stresses. (*b*) Wall-normal behavior of the total ($q_{ad}^{tot}$), turbulent ($q_{ad}^{t}$), and conductive ($q_{ad}^{v}$) heat fluxes.**

flow. Here, we deepen those results by looking at the wall-normal behavior of both the shear stress (wall-normal transport of momentum) and the heat flux (wall-normal transport of heat). Further statistics of flow velocity and temperature fluctuations are presented in Appendix. In Fig. 8(*a*), we consider the wall-normal shear stress, $(\tau_{xz}/\rho u_\tau^2) = \tau_{xz}^v + \tau_{xz}^t$, where $\tau_{xz}^v = (1/\mathrm{Re}_\tau)(\partial\langle u_x\rangle/\partial z)$ is the viscous shear stress and $\tau_{xz}^t = \langle u_x' u_z'\rangle$ is the turbulent shear stress ($u_i'$ being the fluid velocity fluctuations). As expected, the total shear stress does not change between the different simulations (our simulations are performed imposing the same pressure gradient, i.e., the same total shear stress) and is a straight line between $\tau_{xz} = 1$ (at the wall) and $\tau_{xz} = 0$ (at the channel centerline). However, the relative importance of the turbulent and viscous stresses to the total stress changes between the different cases. Compared to the reference case of forced convection turbulence (symbols), $\tau_{xz}^t$ increases for PRB flow (solid line) and increases even further when $\beta(T)$ is considered (dash-dotted line). Corresponding to the increase of $\tau_{xz}^t$, the viscous shear stress $\tau_{xz}^v$ decreases (to keep the total shear stress constant). This confirms that the wall-normal transport of momentum is efficiently driven by turbulent fluctuations induced by buoyancy. In Fig. 8(*b*), we consider the wall-normal heat flux $(q/(\rho c_p u_\tau \Delta T_{HC}/2)) = q^v + q^t$, where $q^v = (1/\mathrm{PrRe}_\tau)(\partial\langle\theta\rangle/\partial z)$ and $q^t = \langle\theta' u_z'\rangle$ are the diffusive and the turbulent part of the total heat flux, respectively. Heat fluxes are normalized as $q_{ad} = (q/q_{FC})$; $q_{ad}^v = (q^v/q_{FC})$; $q_{ad}^t = (q^t/q_{FC})$, where $q_{FC}$ is the wall-normal heat flux for forced convection turbulence. Compared to $q_{FC}$, the total heat flux for PRB turbulent channel flow (solid line) is higher (+70%). A further increase (+30%) of the total heat flux is observed for $\beta(T)$. Note that the diffusive heat flux $q_{ad}^v$ is very small throughout the entire channel height but in the near wall-region, where higher temperature gradients are observed (see Fig. 7(*b*)). The near wall-region is the region where the effect of buoyancy and of $\beta(T)$ on $q_{ad}^v$ is clearly visible. Different conclusions can be drawn for the turbulent heat flux $q_{ad}^t$. Large variations of $q_{ad}^t$ are found throughout the entire channel height and confirm the observation that the wall-normal transport of heat is carried by turbulent fluctuations of velocity (driven by buoyancy).

**3.6 Mixing Efficiency in PRB Turbulent Channel Flow.** We conclude our analysis with the computation of mixing efficiency in PRB turbulent channel flow. The key question we want to address is how mixing efficiency is modified by the amount of buoyancy. Mixing efficiency may be evaluated using the flux Richardson number $Ri_f$ [30–32]

$$Ri_f = \frac{B_k}{P_k} = \frac{\frac{Ri_\tau}{16}\langle\theta' u_z'\rangle}{\langle u_x' u_z'\rangle \frac{\partial\langle u_x\rangle}{\partial z}} \tag{9}$$

where $B_k$ and $P_k$ are production of TKE by buoyancy and by mean shear, respectively. Mixing efficiency quantifies the amount of TKE (i.e., energy available for mixing) lost to potential energy (PE). For PRB flows, PE generates TKE, hence $Ri_f$ is negative. Here, we consider the absolute value of the flux Richardson number. The behavior of $Ri_f$ as a function of the wall-normal coordinate is given in Fig. 9(*a*) for the three different Richardson (and Reynolds) numbers and for OB approximation. Consider first the behavior of $Ri_f$ for a given Richardson (or Reynolds) number: $Ri_f$ increases rapidly while moving from the wall to the center of the channel. This behavior may be explained by looking at the contribution of $B_k$ and $P_k$ to $Ri_f$ (Figs. 9(*b*) and 9(*c*), respectively). In PRB turbulent channel flow both production of TKE by buoyancy ($B_k$) and by mean shear ($P_k$) are usually important, but not in the same place [3]. Production of TKE by mean shear (Fig. 9(*b*)) is more intense near the surface (and falls of strongly away from the surface), while production of TKE by buoyancy (Fig. 9(*c*)) is very important far from the near-wall region. As a consequence, (i) $Ri_f$ is large in the core of the channel (where, owing to $(\partial\langle u_x\rangle/\partial z) \to 0$, $P_k$ is small and $B_k$ is large) while (ii) $Ri_f$ is small in the near wall region (where $P_k$ is large and $B_k$ is small). Where $Ri_f$ is large, turbulence (TKE) is efficiently produced by buoyancy ($B_k$) rather than by mean shear ($P_k$). The trend of mixing efficiency for increasing Richardson (and Reynolds) number is explicitly indicated by arrows in Fig. 9(*a*). As expected, mixing efficiency increases for increasing $Ri_\tau$ and decreases for increasing $Re_\tau$. For increasing $Ri_\tau$, turbulence production by buoyancy ($B_k$) increases and the corresponding mixing efficiency increases. For increasing $Re_\tau$, the relative importance of turbulence production by buoyancy ($B_k$) decreases as well as the corresponding mixing efficiency.

Finally, we consider the effect of $\beta(T)$ on mixing efficiency. To this aim, we compute the ratio $Ri_{f,\beta}/Ri_f$, where $Ri_{f,\beta}$ is the mixing efficiency for simulations with $\beta(T)$. Results are shown in Fig. 9(*d*). For each Richardson number, $\beta(T)$ increases the mixing efficiency of the flow ($Ri_{f,\beta}/Ri_f > 1$ everywhere but in a small region near the wall). However, the effect of $\beta(T)$ is higher in the buffer region ($Ri_{f,\beta}/Ri_f > 1.5$) and lower in the core region ($1 < Ri_{f,\beta}/Ri_f < 1.5$), indicating that mixing efficiency is selectively modified by $\beta(T)$, with a maximum impact in the buffer

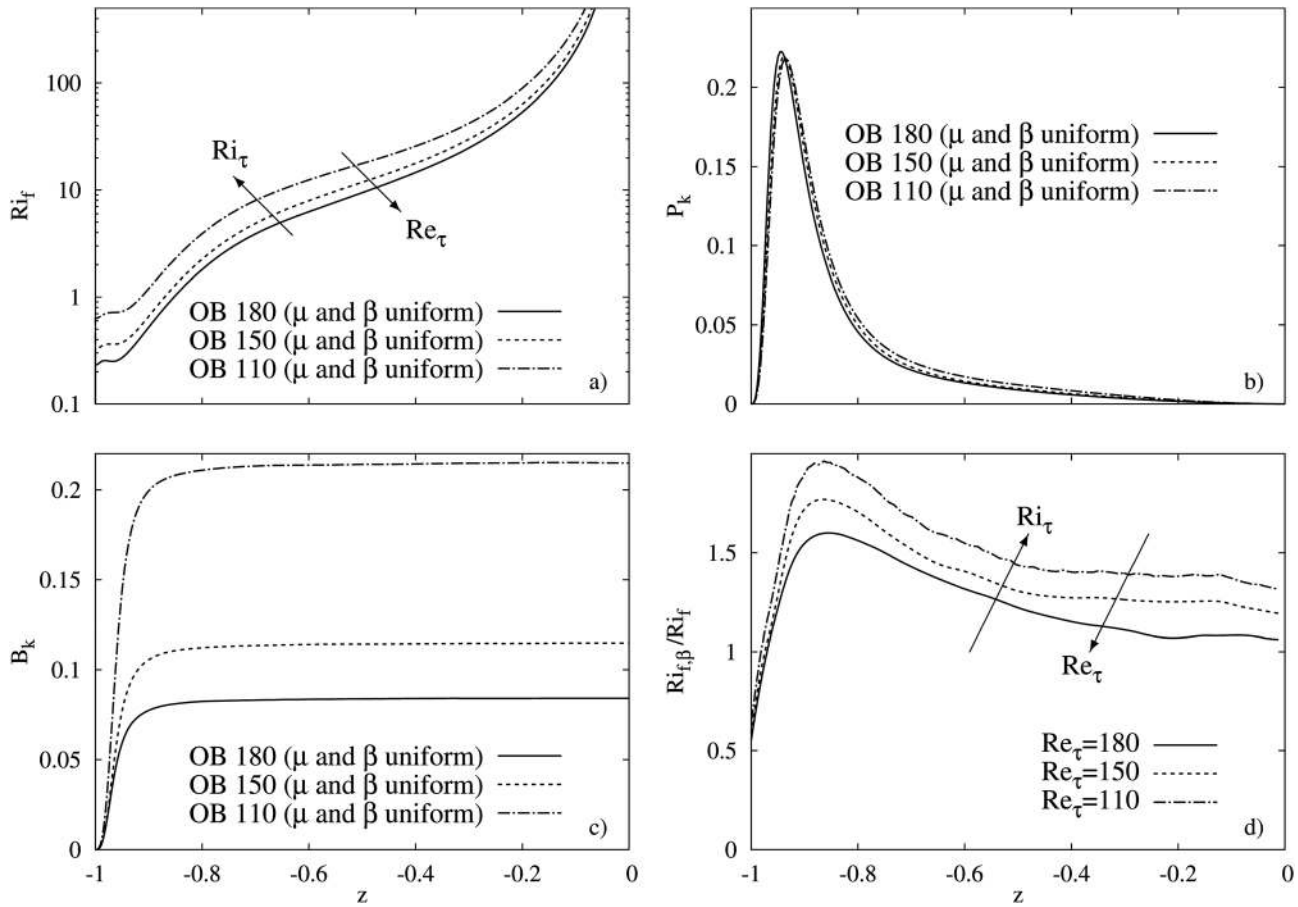


**Fig. 9 (a) Mixing efficiency ($Ri_f$) for PRB turbulent channel flow (assuming OB conditions) at Richardson number $Ri_\tau = 346$ ($Re_\tau = 180$, solid line), $Ri_\tau = 498$ ($Re_\tau = 150$, dotted line), and $Ri_\tau = 926$ ($Re_\tau = 110$, dash-dotted line). (*b*) Production of TKE by mean shear, $P_k$. (*c*) Production of TKE by buoyancy, $B_k$. (*d*) Wall-normal behavior of the ratio between mixing efficiency for PRB turbulent channel flow assuming temperature-dependent thermal expansion coefficient ($Ri_{f,\beta}$) and the mixing efficiency for PRB turbulent channel flow assuming uniform fluid properties ($Ri_f$).**

region (where buoyancy effects are predominant). The trend of $Ri_{f,\beta}/Ri_f$ for increasing $Ri_\tau$ is indicated by arrows in Fig. 9(*d*). We note the tendency for $Ri_{f,\beta}/Ri_f$ to be increased for increasing $Ri_\tau$, and decreased for increasing $Re_\tau$. This is consistent with the results discussed in Sec. 3.5, where we observed that $\beta(T)$ increases the wall normal transport of turbulence fluctuations.

## 4 Conclusions

Mixing in PRB turbulent channel flow is a complex phenomenon, which is crucial in a number of industrial and environmental applications. Further complexity is introduced when OB assumptions are dropped and fluid properties are forced to depend on temperature (NOB): this is the case of turbulent water flows subjected to large temperature gradients. In this paper, the importance of the usual OB approximation in turbulent PRB flow is established via DNS of water flows with fluid viscosity ($\mu$) and thermal expansion coefficient ($\beta$) purely varying with temperature (NOB). DNS are performed using a pseudo-spectral method for the time integration of momentum and energy equations (written in their variable-viscosity/thermal expansion coefficient formulation) for the case of PRB water channel flows.

Flow simulations (either with uniform or with temperature-dependent fluid properties) were run at reference Prandtl number $Pr = 3$ and at three different absolute values of the shear Richardson number $Ri_\tau = 926$, 498, and 346 (corresponding to shear Reynolds numbers $Re_\tau = 110$, 150, 180, and Grashof number $Gr = 1.12 \times 10^7$). Fluid velocity and temperature statistics obtained from simulations of PRB turbulent channel flow assuming OB and NOB conditions have been compared with those relative to the reference case of forced convection turbulence. Discussion has been done with reference to the simulations at $Ri_\tau = 498$. For PRB turbulent flow, thermal convection induced by buoyancy increases the wall-normal transport of momentum and heat compared to the corresponding forced convection turbulence, where temperature is a passive scalar. We have found that only the effect of $\beta(T)$ is important, whereas the effect of $\mu(T)$ is negligible. For simulations of PRB flow with $\beta(T)$, the wall-normal transport of momentum and heat increases compared to that obtained assuming OB approximation. We have provided a qualitative explanation of the observed statistical behavior by examining the instantaneous flow structure. One of the key features of PRB turbulent channel flow is the generation of large-scale circulation, which has no counterpart in forced convection turbulence. The dynamics of large scale circulation may be explained as follows: (i) large scale convection is triggered by thermal plumes arising from the near wall region; (ii) the hot and cold plumes (which are separated laterally) exert buoyancy forces to the bulk fluid and drive the flow in the vertical direction; (iii) the vertical flow reaches the opposite wall where it is deflected in the horizontal direction, pushing newly forming plumes closer (cluster of plumes); (iv) the process is self-feeding and starts again. Frequency spectra (of fluid velocity fluctuations) have been used to detect large scale motions (low wave number events) occurring for PRB turbulent flow. A simplified phenomenological model of heat transfer in PRB turbulent flows, based on the assumption that heat is carried primarily by thermal plumes and near-wall bursting events, has been developed. Finally, we have

computed the mixing efficiency of the flow: calculations have been performed for each Reynolds (and Richardson) number, to observe possible trends in the $\mathrm{Re}_\tau$ (or $\mathrm{Ri}_\tau$) parameter space. We have observed that (i) mixing efficiency increases for increasing $\mathrm{Ri}_\tau$ (and decreases for increasing $\mathrm{Re}_\tau$) and (ii) the effect of temperature-dependent thermal expansion coefficient on mixing efficiency is larger for increasing $\mathrm{Ri}_\tau$ (and is weaker for increasing $\mathrm{Re}_\tau$).


## Acknowledgment

CINECA supercomputing center (Bologna, Italy) and DEISA Extreme Computing Initiative are gratefully acknowledged for generous allowance of computer resources. Support from PRIN (under Grant No. 2006098584_004) and from HPC Europa Transnational Access Program (under Grant Nos. 466 and 708) are gratefully acknowledged. Part of this work was carried out by F.Z. at EPFL (Lausanne) in the group of Professor J. R. Thome, whose useful remarks and hospitality are gratefully acknowledged.


## Nomenclature

$\mathrm{Nu}_b$ = bulk Nusselt number
$\mathrm{Re}_b$ = bulk Reynolds number
$T_b$ = bulk temperature
$\beta_{\mathrm{bulk}}$ = bulk thermal expansion coefficient
$u_b$ = bulk velocity
$\mathrm{Nu}_c$ = centerline Nusselt number
$\rho$ = density
$q_w$ = diffusive heat flux at the wall
$q^v$ = diffusive part of the wall-normal heat flux
$\theta$ = dimensionless fluid temperature
$\mu$ = dynamic viscosity
$\theta'$ = fluid temperature fluctuation
$u'_x, u'_y, u'_z$ = fluid velocity fluctuations in x, y and z directions
$\mathrm{Ri}_f$ = flux Richardson number (absolute value)
Gr = Grashof number
$C_f$ = friction factor
$g$ = gravitational acceleration
$h$ = half channel height
$Q_1$ = heat transferred from the wall by a submerged jet (phenomenological model)
$\alpha$ = heat transfer coefficient
$\nu$ = kinematic viscosity
$T_{\mathrm{ref}} = (T_H + T_C)/2$ = mean reference temperature
Nu = Nusselt number
Pr = Prandtl number
$p$ = pressure
$\mathrm{Re}_\tau$ = shear Reynolds number
$\mathrm{Ri}_\tau$ = shear Richardson number (absolute value)
$u_\tau$ = shear velocity
$L_x, L_y, L_z$ = size of the computational domain in $x$, $y$, and $z$ directions
$E_{u_i^2}$ = spanwise energy spectra of fluid velocity fluctuations
$c_p$ = specific heat
$T$ = temperature
$\Delta T_{HC}$ = temperature difference between the hot and cold walls
$T_H$ = temperature of the hot (bottom) wall
$T_C$ = temperature of the cold (top) wall
$\beta$ = thermal expansion coefficient
$\lambda$ = thermal conductivity
$q^t$ = turbulent part of the wall-normal heat flux
$\tau^t_{xz}$ = turbulent part of the wall-normal shear stress
$w_m, T_m$ = velocity and temperature at the axis of the jet (phenomenological model)
$w_{m,\mathrm{burst}}$ = velocity at the axis of the jet due to bursts (phenomenological model)
$w_{m,\mathrm{plume}}$ = velocity at the axis of the jet due to plumes (phenomenological model)
$\tau^v_{xz}$ = viscous part of the wall-normal shear stress
$\tau_w$ = viscous shear stress at the wall
$q_{\mathrm{FC}}$ = wall normal heat flux for turbulent forced convection
$\tau_{xz}$ = wall-normal shear stress
$T_W$ = wall temperature made symmetrical with respect to the reference temperature
$k$ = wave number (along $y$ direction)

## Superscripts and Subscripts

$\langle\rangle$ = average in time and in space (over the homogeneous directions)
$+$ = nondimensionalized by $u_\tau$ and $\nu$
$-$ = nondimensionalized by $u_\tau$ and $h$
ad = nondimensionalized by the wall-normal heat flux for forced convection
RMS() = root mean square value
0 = value computed for $\mathrm{Gr} = 0$, i.e., in turbulent forced convection
$H, C$ = value computed at the hot and cold walls
ref = variable computed at the reference temperature $T_{\mathrm{ref}} = (T_H + T_C)/2$

## Appendix: Turbulence Statistics

The root mean square (RMS) of the fluid velocity fluctuations (in each direction), $\langle \mathrm{RMS}(u'_i)\rangle$, and of the fluid temperature fluctuations, $\langle \mathrm{RMS}(\theta')\rangle$, is shown in Fig. 10. Since the flow asymmetry induced by NOB conditions is low compared to the overall effect produced by buoyancy, we will present flow statistics for half domain only (average has been done between the results for $-1 < z < 0$ and those for $0 < z < 1$). To analyze those effects induced by stratification only, we begin from the comparison between the case of PRB turbulent channel flow assuming OB approximation (solid line) and the reference case of forced convection turbulence (symbols). As buoyancy effects appear, streamwise fluctuations ($\langle \mathrm{RMS}(u'_x)\rangle$, Fig. 10(*a*)) increase in the core region of the channel (mixing enhancement) but decrease in the buffer region. By contrast, spanwise ($\langle \mathrm{RMS}(u'_y)\rangle$, Fig. 10(*b*)) and wall-normal velocity fluctuations ($\langle \mathrm{RMS}(u'_z)\rangle$, Fig. 10(*c*)) increase along the whole channel height. In particular, $\langle \mathrm{RMS}(u'_y)\rangle$ increases very sharply in the near-wall region, reaches a maximum at $z \simeq -0.85$ and decreases up to the channel centerline ($z = 0$); differently, $\langle \mathrm{RMS}(u'_z)\rangle$ increases monotonically from the channel wall up to the channel centerline, where it reaches its maximum. The increase of $\langle \mathrm{RMS}(u'_y)\rangle$ and $\langle \mathrm{RMS}(u'_z)\rangle$ indicates the activation of cross-stream eddies generated from the thermal plumes raising up from each wall (see Sec. 3.2). Root mean square of temperature fluctuations, $\langle \mathrm{RMS}(\theta')\rangle$, are shown in Fig. 10(*d*). It is clear that $\langle \mathrm{RMS}(\theta')\rangle$ decreases in the core of the channel for PRB flow, indicating the tendency for temperature fluctuations to be damped (mixing is more effective and temperature fluctuations are more homogeneously distributed). Whereas the effects of $\mu(T)$ on velocity and temperature fluctuations are negligible (solid lines and dotted lines coincide), the influence of $\beta(T)$ is strong: for NOB assumption, streamwise velocity fluctuations $\langle \mathrm{RMS}(u'_x)\rangle$ decrease in the buffer region, but increase in the core region of the channel (Fig. 10(*a*)). Spanwise ($\langle \mathrm{RMS}(u'_y)\rangle$) and wall-normal ($\langle \mathrm{RMS}(u'_y)\rangle$) velocity fluctuations increase along the whole channel height (Figs. 10(*b*) and 10(*c*)), while temperature fluctuations ($\langle \mathrm{RMS}(\theta')\rangle$) decrease throughout the whole channel height but in the near wall region (Fig. 10(*d*)). All the previous observations

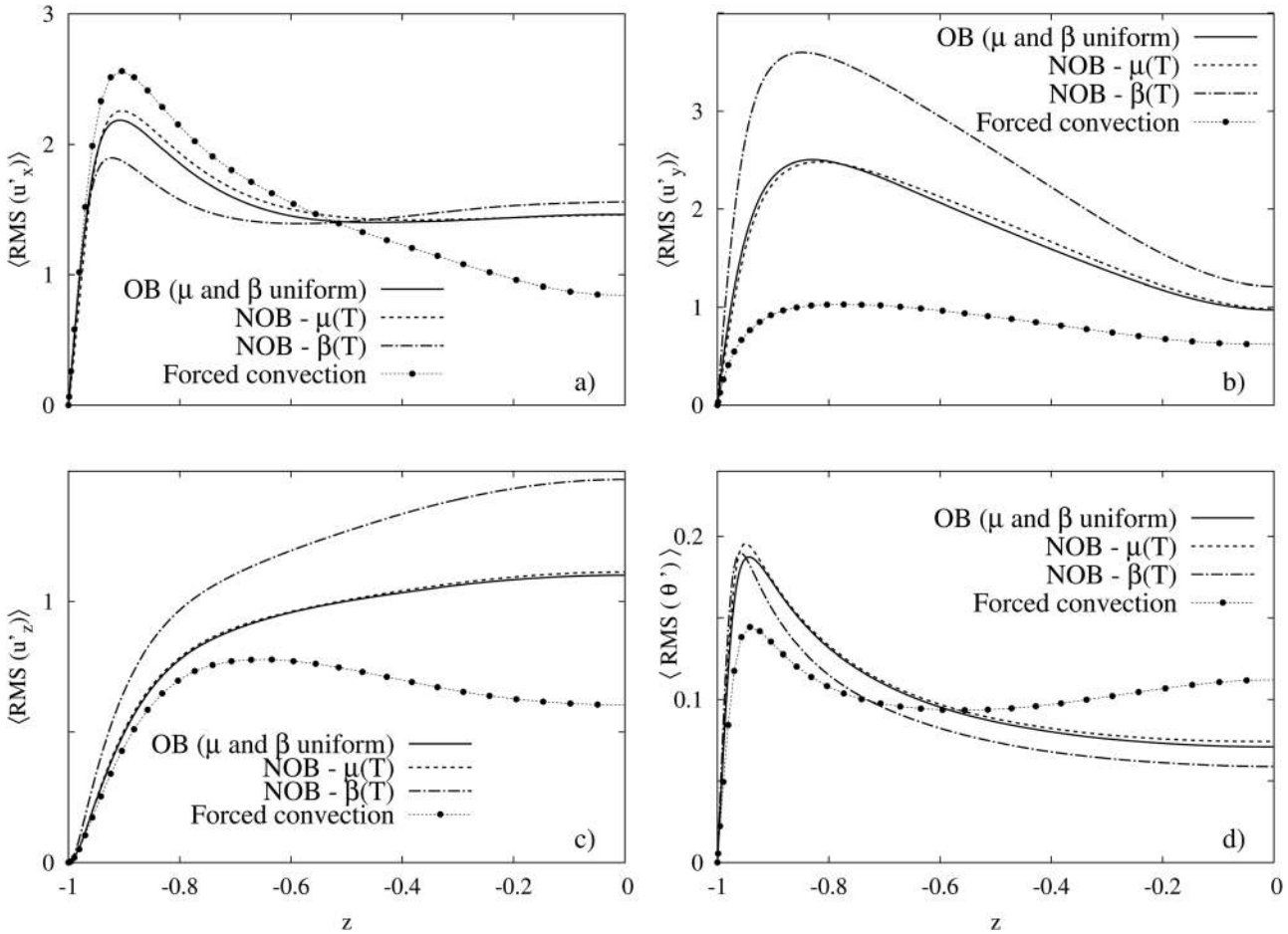


**Fig. 10 Fluid velocity and temperature statistics for PRB turbulent channel flow at $Ri_\tau = 498$ ($Re_\tau = 150$): comparison between simulations with uniform thermophysical properties (OB, solid line) and simulations with temperature-dependent viscosity (NOB, dashed line) and temperature-dependent thermal expansion coefficient (NOB, dash-dotted line). Results from the simulation of forced convection turbulence (symbols) are also included. (*a*) RMS of streamwise velocity fluctuations, $\langle \mathrm{RMS}(u_x') \rangle$; (*b*) RMS of spanwise velocity fluctuations, $\langle \mathrm{RMS}(u_y') \rangle$; (*c*) RMS of wall-normal velocity fluctuations, $\langle \mathrm{RMS}(u_z') \rangle$; (*d*) RMS of temperature fluctuations, $\langle \mathrm{RMS}(\theta') \rangle$.**

indicate that $\beta(T)$ has a strong impact on momentum and heat transport efficiency, whereas $\mu(T)$ has only negligible effects (for this flow configuration).

Higher wall-normal velocity fluctuations for $\beta(T)$ can be explained considering that the buoyancy force acting on a fluid particle is proportional to the local value of the thermal expansion coefficient, $F_B \sim \beta(z)$. Since $\beta(T)$ is a monotonic function of temperature, compared to OB approximation, NOB assumption increases the buoyancy of a fluid parcel at the hot wall and decreases the buoyancy of a fluid parcel at the cold wall. Altogether, they result in an increase of fluctuations, mixing and wall-normal transport of momentum and heat. We found good agreement between the trend of our results and that reported by Sameen et al. [33], even though obtained in different flow configurations (PRB turbulent channel flow in our work, Rayleigh-Bénard convection in Sameen et al. [33]).

## References


[1] Wang, M., Fu, S., and Zhang, G., 2002, "Large-Scale Spiral Structures in Turbulent Thermal Convection Between Two Vertical Plates," Phys. Rev. E, **66**, p. 066306.

[2] Hartmann, D. L., Moy, L. A., and Fu, Q., 2001, "Tropical Convection and the Energy Balance at the Top of the Atmosphere," J. Climate, **14**, pp. 4495–4511.

[3] Lumley, J. L., Zeman, O., and Siess, J., 2009, "The Influence of Buoyancy on Turbulent Transport," J. Fluid Mech., **84**, pp. 581–597.

[4] Incropera, F. P., and Dewitt, D. P., 1985, *Fundamentals of Heat and Mass Transfer*, John Wiley and Sons Inc., New York.

[5] Sugiyama, K., Calzavarini, E., Grossmann, S., and Lohse, D., 2009, "Flow Organization in Two-Dimensional Non-Oberbeck-Boussinesq Rayleigh-Benard Convection in Water," J. Fluid Mech., **637**, pp. 105–135.

[6] Timchenko, V., 2012, "Eddie Leonardi Memorial Lecture: Natural Convection From Earth to Space," ASME J. Heat Transfer, **134**, p. 031014.

[7] Zonta, F., Marchioli, C., and Soldati, A., 2011, "Time Behavior of Heat Fluxes in Thermally Coupled Turbulent Dispersed Particle Flows," Acta Mech., **218**, pp. 367–373.

[8] Lee, J., Gharagozloo, P. E., Kolade, B., Eaton, J. K., and Goodson, K. E., 2010, "Nanofluid Convection in Microtubes," ASME J. Heat Transfer, **132**, p. 092401.

[9] Arcen, B., Taniere, A., and Khalij, M., 2012, "Heat Transfer in a Turbulent Particle-Laden Channel Flow," Int. J. Heat Mass Transfer, **55**, pp. 6519–6529.

[10] Ahlers, G., Grossmann, S., and Lohse, D., 2009, "Heat Transfer and Large Scale Dynamics in Turbulent Rayleigh-Benard Convection," Rev. Mod. Phys., **81**, pp. 503–537.

[11] Verzicco, R., and Camussi, R., 2003, "Numerical Experiments on Strongly Turbulent Thermal Convection in a Slender Cylindrical Cell," J. Fluid Mech., **477**, pp. 19–49.

[12] Xia, C., and Murthy, J. Y., 2002, "Buoyancy Driven Flow Transitions in Deep Cavities Heated From Below," ASME J. Heat Transfer, **124**, pp. 650–659.

[13] Komori, S., Ueda, H., Ogino, F., and Mizushina, T., 1982, "Turbulence Structures in Unstably-Stratified Open-Channel Flow," Phys. Fluids, **25**, pp. 1539–1546.

[14] Fukui, K., and Nakajima, M., 1985, "Unstable Stratification Effects on Turbulent Shear Flow in the Wall Region," Int. J. Heat Mass Transfer, **28**, pp. 2343–2352.

[15] Fukui, K., Nakajima, M., and Ueda, H., 1991, "Coherent Structure of Turbulent Longitudinal Vortices in Unstably-Stratified Turbulent Flow," Int. J. Heat Mass Transfer, **34**, pp. 2373–2385.

[16] Domaradzki, J. A., and Metcalfe, P. W., 1988, "Direct Numerical Simulations of the Effects of Shear on Turbulent Rayleigh-Benard Convection," J. Fluid Mech., **193**, pp. 499–531.

[17] Iida, O., and Kasagi, N., 1997, "Direct Numerical Simulation of Unstably Stratified Turbulent Channel Flow," ASME J. Heat Transfer, **119**, pp. 53–67.
[18] Zainali, A., and Lessani, B., 2010, "Large-Eddy Simulation of Unstably Stratified Turbulent Channel Flow With High Temperature Differences," Int. J. Heat Mass Transfer, **53**, pp. 4865–4875.
[19] Zonta, F., Marchioli, C., and Soldati, A., 2012, "Modulation of Turbulence in Forced Convection by Temperature-Dependent Viscosity," J. Fluid Mech., **697**, pp. 150–174.
[20] Zonta, F., Onorato, M., and Soldati, A., 2012, "Turbulence and Internal Waves in Stably-Stratified Channel Flow With Temperature-Dependent Fluid Properties," J. Fluid Mech., **697**, pp. 175–203.
[21] Kerr, R., and Herring, J. R., 2000, "Prandtl Number Dependence of Nusselt Number in Direct Numerical Simulations," J. Fluid Mech., **419**, pp. 325–344.
[22] Parodi, A., von Hardenberg, J., Passoni, G., Provenzale, A., and Spiegel, E. A., 2004, "Clustering of Plumes in Turbulent Convection," Phys. Rev. Lett., **92**, p. 194503.
[23] Dean, R. B., 1978, "Reynolds Number Dependence of Skin Friction and Other Bulk Flow Variables in Two-Dimensional Rectangular Duct Flow," ASME J. Fluid Eng., **100**, pp. 215–223.
[24] Sieder, E. N., and Tate, G. E., 1936, "Heat Transfer and Pressure Drop of Liquids in Tubes," Ind. Eng. Chem., **28**, pp. 1429–1435.
[25] Perry, A., and Chong, M. S., 1987, "A Description of Eddying Motions and Flow Patterns Using Critical Point Concepts," Annu. Rev. Fluid Mech., **9**, pp. 125–155.
[26] Schoppa, W., and Hussain, F., 2002, "Coherent Structure Generation in Near-Wall Turbulence," J. Fluid Mech., **453**, pp. 57–108.
[27] Xi, H., Lam, S., and Xia, K., 2004, "From Laminar Plumes to Organized Flows: The Onset of Large Scale Circulation in Turbulent Thermal Convection," J. Fluid Mech., **503**, pp. 47–56.
[28] Hetsroni, G., Yarin, L. P., and Kaftori, D., 1996, "A Mechanistic Model for Heat Transfer From a Wall to a Fluid," Int. J. Heat Mass Transfer, **39**, pp. 1475–1478.
[29] Schlichting, H., 1979, *Boundary Layer Theory*, McGraw-Hill, New York.
[30] Peltier, W. R., and Caulfield, C. P., 2003, "Mixing Efficiency in Stratified Shear Flows," Annu. Rev. Fluid Mech., **35**, pp. 135–167.
[31] Fernando, H. J. S., 1991, "Turbulent Mixing in Stratified Fluids," Annu. Rev. Fluid Mech., **23**, pp. 455–493.
[32] Lawrie, A. G. W., and Dalziel, S. B., 2011, "Rayleigh-Taylor Mixing in an Otherwise Stable Stratification," J. Fluid Mech., **688**, pp. 507–527.
[33] Sameen, A., Verzicco, R., and Sreenivasan, K. R., 2009, "Specific Role of Fluid Properties in Non-Boussinesq Thermal Convection at the Rayleigh Number of $2 \times 10^8$," Europhys. Lett., **86**, p. 14006.